Dry Surface Frontogenesis Arising from Interior Potential Vorticity Perturbations in a Semigeostrophic Model

MICHAEL T. MONTGOMERY AND BRIAN F. FARRELL

Department of Earth and Planetary Sciences, Harvard University, Cambridge, Massachusetts

(Manuscript received 6 June 1989, in final form 15 March 1990)

ABSTRACT

We examine the role of interior potential vorticity perturbations in surface frontogenesis using the two-dimensional semigeostrophic Eady model. Fronts form rapidly for properly configured small disturbances even at zonal wavenumbers for which no exponentially unstable modes exist. While lack of exponential growth does not preclude frontal development, the strength of the disturbance must exceed an amplitude threshold for frontal formation. In practice, the finite amplitude constraint is not severe requiring meridional winds of a few meters per second.

Model integrations illustrate the variety of frontogenesis phenomena that arise from interior potential vorticity perturbations including formation of near surface vertical velocity maxima.

1. Introduction

A ubiquitous feature of large scale atmospheric weather systems at midlatitudes is surface concentrated zones of sharp transition in velocity and temperature called fronts. These fronts have velocity and temperature contrasts ranging from a few to as much as 50 m s^{-1} associated with temperature contrasts of up to 20 K. The across-front scale is typically much smaller than the along-front scale with 10 km and 1000 km, respectively, being representative. Frequently fronts become indistinct a few kilometers above the surface; however, there are cases of fronts that have been observed to extend through the depth of the atmosphere (Sanders 1983). The fronts considered in this paper are surface concentrated.

Originally the front was viewed as a discontinuity in temperature and velocity, and this idea formed the basis of the polar front model advanced by the Norwegian school (Bjerknes 1919). In this model the large scale eddies of the atmosphere were thought to develop on the front in analogy with the Kelvin-Helmholtz instability. Upper-air observations made in the 1930s and 1940s revealed continuous sloping zones of rapid transition in temperature and velocity fields rather than discontinuities (Bjerknes and Palmen 1937; Palmen and Newton 1948). These and later observations of surface fronts by Sanders (1955) gave an entirely different picture than that suggested by the polar front model.

Building on observational advances in the gathering of upper air data were advances in theoretical understanding of basic energy conversions in continuously stratified rotating fluid systems. The demonstration by Eady (1949) and Charney (1947) that such fluids possess hydrodynamic instabilities proved fundamental to understanding the origin and development of cyclones. Fronts associated with cyclones are now viewed as consequences of baroclinic wave intensification. Thus, the original idea that cyclones developed on fronts was replaced by the idea that fronts arise as a result of intensifying cyclones.

Frontogenesis in association with an intensifying baroclinic wave was examined by Williams (1967) using a primitive equation model and this simulation exhibited rapid frontal collapse and possessed a sloping cross-frontal circulation. This work showed that the primitive equations are sufficient to capture the physics of frontogenesis, but the awkwardness of working with the full equations motivated the search for a balance approximation that would provide equations containing the essential frontogenetic mechanism. Hoskins and Bretherton (1972) developed such a system, which is referred to as the semigeostrophic equations. Using this approximate equation set, they investigated both the deformation and baroclinic wave frontogenetic mechanisms and found rapid formation of fronts and sloping cross-frontal circulations in agreement with primitive equation simulations.

In this work the frontogenetic process associated with a growing baroclinic wave is examined as an initial value problem. The standard paradigm for understanding baroclinic instability in the atmosphere results in an eigenvalue problem for the growth rates and eigenfunctions of unstable normal modes (Charney

Corresponding author address: Dr. Michael Montgomery, Dept. of Earth and Planetary Sciences, Harvard University, Cambridge, MA 02138.

1947; Eady 1949); an approach that focuses attention entirely on individual unstable normal modes. In the Eady model the exponential normal modes are sufficient to represent all disturbances with uniform potential vorticity. In this special case, Williams (1967), Hoskins and Bretherton (1972), Hoskins (1975) and Hoskins and West (1979) studied baroclinic wave frontogenesis. Recently, however, Farrell (1984) has stressed the importance of the transient growth phase of baroclinic development in which the potential vorticity is not uniform in the Eady model and has argued that explosive cyclogenesis results from transient processes. Expressed in a modal context, transient growth comes about through a cooperative interaction between all the modes and looking only at single modes, such as the most unstable mode, is highly restrictive. The distinction between these mechanisms for growth of baroclinic waves persists in the frontogenetic context in which the dynamics is essentially nonlinear. Interior potential vorticity gradients have long been associated with cyclogenesis (Eliassen and Kleinschmidt 1957; Hoskins et al. 1985) and this role is becoming more widely appreciated (Hoskins et al. 1985). In this work, surface frontogenesis with interior potential vorticity perturbations is examined within the framework of a two-dimensional semigeostrophic Eady model.

2. Model formulation and description

The flows considered are dry and inviscid with time scales long compared to gravity and acoustic wave periods. This separation of time scales justifies filtering the gravity wave modes by using a balance approximation. The semigeostrophic equations are adopted as being less restrictive than the quasi-geostrophic approximation, while retaining advection by the ageostrophic wind fields. Retaining these advections is known to produce frontal features characterized by an infinite relative vorticity and collapsed isotherms at the vertical boundaries in a finite period of time (Williams 1967; Hoskins and Bretherton 1972). In contrast, quasi-geostrophic models are able to produce surface fronts of finite vorticity in finite time. The rapidity of the frontal formation process is often considered to be of key importance and a fundamental reason for choosing the semigeostrophic balance approximation. The semigeostrophic approximation used here is based on the work of Hoskins and Draghici (1977).

In this work we anticipate meridionally elongated frontal zones with coriolis forces induced by meridional flow along the front geostrophically balanced against cross-frontal pressure gradients. Accelerations along the front are not small compared to coriolis forces induced by cross-frontal flow. The governing equations for inviscid adiabatic flow that is Boussinesq and hydrostatic are:

$$fv_g = \frac{\partial \phi}{\partial x}, \tag{2.1a}$$

$$\frac{\partial v_g}{\partial t} + (u_g + u_{ag})\frac{\partial v_g}{\partial x} + v_g\frac{\partial v_g}{\partial y} + w\frac{\partial v_g}{\partial z} + f(u_g + u_{ag}) = -\frac{\partial \phi}{\partial y}, \tag{2.1b}$$

$$\frac{g\theta}{\theta_0} = \frac{\partial \phi}{\partial z}, \tag{2.1c}$$

$$\frac{\partial u_{ag}}{\partial x} + \frac{\partial w}{\partial z} = 0, \tag{2.1d}$$

$$fu_g = -\frac{\partial \phi}{\partial y}, \tag{2.1e}$$

$$\frac{\partial \theta}{\partial t} + (u_g + u_{ag})\frac{\partial \theta}{\partial x} + v_g\frac{\partial \theta}{\partial y} + w\frac{\partial \theta}{\partial z} = 0, \tag{2.1f}$$

where ϕ is the geopotential, $\theta = T(p_s/p)^{R/c_p}$ the potential temperature, θ_0 a constant reference potential temperature, $z = (c_p\theta_0/g)[1 - (p_s/p)^k]$, where $k = (\gamma - 1)/\gamma$, a vertical coordinate nearly equal to height in the troposphere and γ the ratio of specific heats. Here, u_g and v_g denote the geostrophic wind fields, and u_{ag}, v_{ag} and w denote the ageostrophic wind fields.

The two-dimensional Eady model is a useful simplification of the above system that results from the restriction to a two-dimensional wave field superimposed upon a hydrostatic basic state consisting of a zonally homogeneous constant shear in thermal wind balance with a constant meridional temperature gradient. Early research (Williams 1967; Hoskins and Bretherton 1972) revealed that this model captured the role of the ageostrophic wind fields in the formation of surface fronts and predicted frontal structures resembling observational data. The model produces the infinite relative vorticities and strong convergent winds at surfaces in finite time that constitute the paradigm for surface frontogenetic processes.

The two-dimensional assumption is restrictive because there is no change in the basic state flow during the development of a disturbance. In this model the basic state acts as an infinite reservoir of potential energy, and the conversion between energy of the basic state and energy in the disturbance field is not limited by the amount of potential energy in the basic state or by modification of the basic state.

The basic state is

$$\bar{U}_g = Sz,$$

$$\bar{V}_g = 0, \quad \bar{U}_{ag} = 0, \quad \bar{V}_{ag} = 0, \quad \bar{W} = 0,$$

$$\bar{\Phi}(y, z) = -fSyz + \frac{N_0^2 z^2}{2} + gz,$$

$$\bar{\Theta}(y, z) = -\frac{\theta_0}{g} fSy + \frac{N_0^2\theta_0}{g} z + \theta_0, \tag{2.2}$$

and exactly satisfies Eqs. (2.1).

The basic state is perturbed with the amplitude of the disturbances not assumed to be small. In accord with the two-dimensionality constraint on the distur-

bance field discussed above, we seek x-periodic solutions to Eqs. (2.1) in the form:

$$U_{\text{total}} = \bar{U}_g + u_{ag}(x, z, t), \tag{2.3a}$$

$$V_{\text{total}} = v_g(x, z, t), \tag{2.3b}$$

$$W_{\text{total}} = w(x, z, t), \tag{2.3c}$$

$$\Theta_{\text{total}} = \bar{\Theta}(y, z) + \theta(x, z, t), \tag{2.3d}$$

$$\Phi_{\text{total}} = \bar{\Phi}(y, z) + \Phi(x, z, t). \tag{2.3e}$$

If we transform the horizontal coordinates (x, y) to the geostrophic coordinates (X, Y) via the relation:

$$X = x + v_g/f,$$

$$Y = y - u_g/f \tag{2.4a}$$

the resulting system of equations simplify considerably since advection by the ageostrophic wind u_{ag} is now implicit in these coordinates and is no longer explicit in the substantial derivative (Eliassen 1962; Hoskins and Bretherton 1972). If we further define a modified geopotential,

$$\Phi = \phi + \tfrac{1}{2} v_g{}^2, \tag{2.4b}$$

the geostrophic and hydrostatic relations (2.1a, 2.1c, and 2.1e) become simple in these coordinates,

$$\frac{g\theta}{\theta_0} = \frac{\partial \Phi}{\partial Z}, \quad f u_g = -\frac{\partial \Phi}{\partial Y}, \quad f v_g = \frac{\partial \Phi}{\partial X}. \tag{2.5}$$

Thus (2.4) constitutes a canonical transformation of the system (2.1). Introducing upper case $Z = z$ and $T = t$ to be in accord with the variables X and Y; substituting (2.3) into the system (2.1); using the potential vorticity equation for Q_g in place of the along front momentum equation and transforming the ageostrophic fields (u_{ag}, w) to the star representation (u^*_{ag}, w^*) results in the following system:

$$\left(\frac{\partial}{\partial T} + SZ\frac{\partial}{\partial X}\right) Q_g + w\frac{\partial}{\partial Z} Q_g = 0, \tag{2.6a}$$

$$\left(\frac{\partial}{\partial T} + SZ\frac{\partial}{\partial X}\right)\theta = \frac{f\theta_0}{g} S v_g, \quad \text{on} \quad Z = 0, 1, \tag{2.6b}$$

$$Q_g = \frac{\dfrac{\partial^2 \Phi}{\partial Z^2} + N_0{}^2}{1 - \dfrac{1}{f^2}\dfrac{\partial^2 \Phi}{\partial X^2}}, \tag{2.6c}$$

$$\frac{\partial}{\partial X}\left(Q_g \frac{\partial \psi}{\partial X}\right) + f^2 \frac{\partial^2 \psi}{\partial Z^2} = -2fS\frac{\partial v_g}{\partial X}. \tag{2.6d}$$

The starred ageostrophic velocities and the unstarred ageostrophic velocities are obtained via the expressions:

$$u^*_{ag} = +\frac{\partial \psi}{\partial Z}, \tag{2.7a}$$

$$w^* = -\frac{\partial \psi}{\partial X}, \tag{2.7b}$$

$$w = Jw^*, \tag{2.7c}$$

$$u_{ag} = u^*_{ag} - \frac{w}{f^2}\frac{\partial^2 \Phi}{\partial Z \partial X}, \tag{2.7d}$$

$$J = \frac{1}{1 - \dfrac{1}{f^2}\dfrac{\partial^2 \Phi}{\partial X^2}}. \tag{2.7e}$$

After solving this system in (X, Z) coordinates, the variables are transformed back to real physical space according to the geostrophic transformation:

$$x = X - \frac{1}{f} v_g(X, Z, T). \tag{2.7f}$$

The J in Eq. (2.7e) denotes the Jacobian of the transformation between the real (x, y) and geostrophic (X, Y) coordinates. It also equals the ratio of the vertical component of absolute vorticity to f:

$$J = 1 + \frac{1}{f}\zeta = 1 + \frac{1}{f}\frac{\partial v_g}{\partial x}.$$

Regions in geostrophic space where J is greater than unity correspond to x-contracted regions in real space; whereas regions where it is less than unity correspond to x-elongated regions in real space.

General solution to the initial value problem (2.6, 2.7) is made difficult by the nonlinearity of the equations. Analytic solutions in terms of known functions have been found for the limited class of problems in which the potential vorticity, Q_g, is uniform throughout the troposphere. This class of problems is briefly reviewed in section 3. Because a general solution for nonuniform potential vorticity has not been found, the method of solution adopted in this paper is computational and an outline of the solution procedure follows.

The system (2.6) is integrated in a zonally periodic rectangular domain bounded in the vertical by rigid lids representing the earth's surface and tropopause. A sketch of the computational domain is given in Fig. 1. The Q_g and θ equations are advanced temporally with

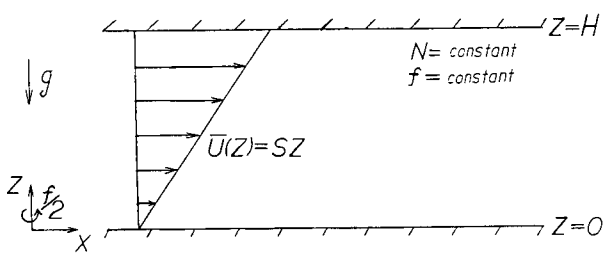

FIG. 1. Sketch of the two-dimensional Eady model geometry defined in section 2.

an Adams-Bashforth predictor-corrector method. An upwinded difference is used for the vertical advection of potential vorticity and centered differences are used on all remaining spatial derivatives. Time increments are typically 15 minutes to insure numerical stability. The elliptic equations (2.6c, 2.6d) are solved via a preconditioned picard iteration scheme of the form,

$$\left(\frac{\partial^2}{\partial X^2}+\frac{\partial^2}{\partial Z^2}\right)G^{(l+1)} = F + K\left[(1-Q_g)\frac{\partial^2 G^{(l)}}{\partial X^2},\cdots\right],$$

with appropriate boundary conditions (discussed below). The sequence $G^{(l)}$, $l = 0, 1, 2, \cdots$, represents successive iterates for ψ or Φ; F represents the nonhomogeneous term for either (2.6c, 2.6d), and K is linear in its arguments. A fast cyclic reduction method is used for the solution of each Poisson equation. With a time increment of 15 minutes, 5 digit accuracy for both Poisson equations is achieved in usually no more than 4 iterations. We use 65 grid points in both horizontal and vertical directions.

Boundary conditions require that all fields remain periodic in X and that the vertical velocity w (and therefore w^*) vanish at the rigid lids $Z = 0$ and $Z = H$ or, equivalently, that the cross-frontal streamfunction ψ be zero on the rigid boundaries. A third condition concerns the inversion of the elliptic equation (2.6c). Evaluating the adiabatic equation on the rigid boundaries ($Z = 0$, $Z = H$) and using the condition that $w^* = 0$ yields an evolution equation for $\theta = (\theta_0/g)(\partial\Phi/\partial Z)$ on the rigid boundaries. The values of θ are then used as Neumann boundary conditions along the rigid boundaries for the solution of (2.6c) for the geopotential Φ. The predicted fields (Q_g, θ) are minimally corrected at each time step to insure solvability of this Neumann problem: solvability is equivalent to enforcing global conservation of potential vorticity.

The initial condition for the integration is a specified geopotential Φ throughout the entire domain, including its values on the rigid lids. The potential vorticity can then be computed via (2.6c). The ageostrophic wind fields, consistent with the initial geopotential, are obtained by inverting (2.6d) for ψ and using the relations given in Eqs. (2.7). The integration proceeds by time-advancing both the potential vorticity and adiabatic equations [(2.6a) and (2.6b), respectively] and then solving the diagnostic equations for the updated geopotential Φ and cross-frontal streamfunction ψ. This process is repeated for each time-step.

Denoting dimensional variables by tildes, our choice of scaling is:

$$\tilde{Q}_g = Q_{g_0}Q_g = N_0^2 Q_g$$
$$\tilde{X} = L_R X = Q_{g_0}^{1/2} H f^{-1} X$$
$$\tilde{Z} = HZ$$
$$\tilde{T} = Q_{g_0}^{1/2} S^{-1} f^{-1} T$$
$$\tilde{U}_g = SHU_g$$
$$\tilde{V}_g = SHv_g$$
$$\tilde{u}_{ag} = SHu_{ag}$$
$$\tilde{w} = Q_{g_0}^{-1/2} fSHw$$
$$\tilde{\Phi} = SQ_{g_0}^{1/2} H^2 \Phi$$
$$\bar{\theta} = \frac{\theta_0}{g} HSQ_{g_0}^{1/2}\theta. \qquad (2.8)$$

A list of representative values for these variables is given in Table 1. Note that L_R is a Rossby deformation radius with the square of the Brunt-Väisälä frequency replaced by the potential vorticity. A unit of nondimensional time corresponds to 9.25 hrs.

The resulting nondimensional system of equations contains the single parameter,

$$\frac{S}{\sqrt{Q_{g_0}}} = \mathrm{Ro} = \frac{1}{\sqrt{\mathrm{Ri}}}.$$

This ratio can be identified with either the Rossby number or the inverse square root of the Richardson number, and for the parameter values in Table 1, the value is Ro = 0.3. Examination of the equations reveals that the parameter dependence of the system on the Rossby number can be eliminated through the following scaling transformation on the geopotential Φ:

$$\hat{\Phi} = \mathrm{Ro}\Phi.$$

Relations between the dimensional fields and the nondimensional (hat) variables are listed in Table 2. For the parameter-free system, the potential temperature scale is 30 K and both the zonal and meridional velocity scale is 100 m s^{-1}, whereas the ageostrophic

TABLE 1. Representative values of parameters for the two-dimensional Eady model given in Eq. (2.8).

$Q_{g_0} = N_0^2 = 10^{-4}$ s^{-2}
$H = 10$ km
$f = 10^{-4}$ s^{-1}
$S = 3$ m s^{-1} km^{-1}
$L_R = Q_{g_0}^{1/2} H f^{-1} = 1000$ km
$U = SH = 30$ m s^{-1}
$u_{ag} = SH = 30$ m s^{-1}
$w = Q_{g_0}^{-1/2} fSH = 30$ cm s^{-1}
$T = L_R U^{-1} = \sqrt{\mathrm{Ri}} f^{-1} = 9.25$ hrs
$\theta = \frac{\theta_0}{g} SHQ_{g_0}^{1/2} = 9$ K
$\Phi = SQ_{g_0}^{1/2} H^2 = 3000$ m^2 s^{-2}

TABLE 2. Relation between dimensional (tilde) fields and nondimensional hatted variables defined in section 2.

$$\tilde{\Phi} = Q_{g0}^{1/2} SH^2 \Phi = \frac{Q_{g0}^{1/2} SH^2}{\mathrm{Ro}} \hat{\Phi} = Q_{g0}^{1/2} H^2 \hat{\Phi} = (10^4 \text{ m}^2 \text{ s}^{-2}) \hat{\Phi}$$

$$\tilde{v}_g = SHv_g = HQ_{g0}^{1/2} \hat{v}_g = (100 \text{ m s}^{-1}) \hat{v}_g$$

$$\tilde{\theta} = \frac{\theta_0}{g} Q_{g0} H \hat{\theta} = (30 \text{ K}) \hat{\theta}$$

$$\tilde{u}_{ag} = SH\tilde{u}_{ag} = (30 \text{ m s}^{-1}) \hat{u}_{ag}$$

$$\tilde{w} = Q_{g0}^{-1/2} fSH\hat{w} = (30 \text{ cm s}^{-1}) \hat{w}$$

velocity scaling for u_{ag} and w remains the same as before, namely 30 m s^{-1} and 30 cm s^{-1}, respectively. We will hereafter drop the hat notation.

The anomalous part of the potential vorticity is best displayed explicitly by writing

$$Q_g = q_g + 1.$$

In terms of the anomalous potential vorticity q_g, the dimensionless equations for the disturbance fields become:

$$\left(\frac{\partial}{\partial T} + Z\frac{\partial}{\partial X}\right) q_g + w\frac{\partial}{\partial Z} q_g = 0, \quad (2.9a)$$

$$\left(\frac{\partial}{\partial T} + Z\frac{\partial}{\partial X}\right)\theta = \frac{\partial \Phi}{\partial X}, \quad \text{on} \quad Z = 0, 1, \quad (2.9b)$$

$$(q_g + 1)\frac{\partial^2 \Phi}{\partial X^2} + \frac{\partial^2 \Phi}{\partial Z^2} = q_g, \quad (2.9c)$$

$$\frac{\partial}{\partial X}\left[(q_g + 1)\frac{\partial \psi}{\partial X}\right] + \frac{\partial^2 \psi}{\partial Z^2} = -2\frac{\partial^2 \Phi}{\partial X^2}. \quad (2.9d)$$

The boundary conditions on the geopotential Φ are that it remain periodic in X and satisfy $\theta = \partial\Phi/\partial Z$ along the horizontal boundaries $Z = 0, 1$. The boundary conditions on the streamfunction ψ are that it be periodic in X and vanish on the horizontal boundaries $Z = 0, 1$.

The dimensionless starred ageostrophic velocities and the unstarred ageostrophic velocities are obtained via the expressions:

$$u_{ag}^* = +\frac{\partial \psi}{\partial Z},$$

$$w^* = -\frac{\partial \psi}{\partial X},$$

$$w = Jw^*$$

$$u_{ag} = u_{ag}^* - w\frac{\partial^2 \Phi}{\partial Z \partial X},$$

$$J = \frac{1}{1 - \dfrac{\partial^2 \Phi}{\partial X^2}}. \quad (2.10)$$

The dimensionless transformation between geostrophic and physical coordinates is

$$x = X - v_g(X, Z, T). \quad (2.10f)$$

Although all dimensionless fluid parameters have been eliminated from (2.9–2.10), the nonlinearity of the system implies that the amplitude of the geopotential Φ will remain an implicit parameter. In addition, the solution will depend on the structure of the initial perturbation. Thus, the general solution has both an amplitude and structural dependence, and it is the objective of this work to explore both dependencies.

3. Normal mode surface frontogenesis reviewed

The traditional Eady problem is recovered from the system (2.9–2.10) under the assumption that q_g is identically zero throughout the flow field and squares of small quantities can be neglected. The approximate Jacobian is unity so there is no advection by the zonal ageostrophic wind field. The resulting equations become

$$\left(\frac{\partial}{\partial T} + Z\frac{\partial}{\partial X}\right)\theta = \frac{\partial \Phi}{\partial X}, \quad \text{on} \quad Z = 0, 1, \quad (3.1a)$$

$$\frac{\partial^2 \Phi}{\partial X^2} + \frac{\partial^2 \Phi}{\partial Z^2} = 0, \quad (3.1b)$$

$$\frac{\partial^2 \psi}{\partial X^2} + \frac{\partial^2 \psi}{\partial Z^2} = -2\frac{\partial^2 \Phi}{\partial X^2}. \quad (3.1c)$$

Boundary conditions on Φ and ψ remain the same. In this limit there is no distinction between geostrophic and physical coordinates, and the starred velocities are equal to the nonstarred velocities.

Solutions to the above system (3.1a, 3.1b) are then sought in the form $\Phi = E(Z)\exp[ik(X - cT)]$ and the resulting system becomes an eigenvalue problem for the eigenfunctions $E(Z)$ and eigenvalues c:

$$\frac{d^2 E}{dZ^2} - k^2 E = 0, \quad (3.2a)$$

$$(Z - c)\frac{dE}{dZ} - E = 0, \quad \text{on} \quad Z = 0, 1. \quad (3.2b)$$

Instability of this flow occurs when the imaginary part of c, denoted hereafter as c_i, is positive. The relationship between c_i and c_r (the real part of c) and the wavenumber k is given in Fig. 2. The salient features to note are

(i) The growth rate kc_i achieves a maximum value of approximately 0.3098 at $k = 1.61$ and the associated mode is called the most unstable mode. This growth rate corresponds to a doubling time scale of $T = 2.24$. In dimensional terms for our choice of parameters this

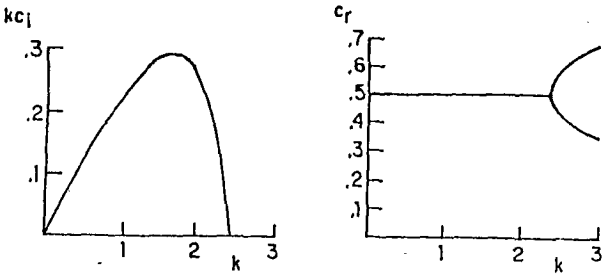

FIG. 2. Phase speed c_r and growth rate c_i as a function of zonal wavenumber k for the normal modes of the Eady problem. All of the Eady normal modes satisfy $q_g \equiv 0$.

corresponds to $T_{\text{dim}} = 20.6$ hours and an approximate X scale of 3900 km.

(ii) The phase speed c_r for the most unstable mode equals 0.5 and corresponds to a dimensional speed of 15 m s^{-1}.

(iii) The wavenumber beyond which no unstable modes exist is approximately $k = 2.4$ and will hereafter be referred to as the short wave cutoff. In dimensional terms, the X scale of the short wave cutoff is approximately 2600 km.

Solutions of the above form can be applied in a more general, nonlinear context by noting that each solution and any linear combination of them also satisfy the full nonlinear equations (2.9–2.10). Superposition of solutions is allowed since the governing equations (3.1) are linear in geostrophic space and it is only in the transformation back to real coordinates

$$x = X - v_g(X, Z, T), \qquad (3.3)$$

that the nonlinearity enters. The advection by u_{ag} is implicit in the coordinate transformation and does not play an active role in the dynamics in geostrophic space.

The classical Eady frontogenesis solution consists of the most unstable normal mode solution. It was first simulated by Williams (1967) with the primitive equations and later with the semigeostrophic equations in geostrophic space by Hoskins and Bretherton (1972). The results of integrating our model with the most unstable mode are presented in Fig. 3. The initial condition used had a maximum surface θ perturbation of 2.22 K and a maximum surface v_g perturbation of 6.3 m s^{-1}.

The computation of all results presented in this paper was terminated when the Jacobian attained a cut-off value. For the most unstable normal mode, a cut-off of $J = 5$ was used, and for the examples discussed in section 4 the cut-off value was $J = 10$. The physical basis for the upper limit on the Jacobian comes from requiring self-consistent solutions to the semigeostrophic system: for the approximation to be valid it is necessary that the local Richardson number be everywhere greater than a quarter. A front with near infinite relative vorticity across it will not satisfy this condition. Despite such a local breakdown of the approximation, the solutions described by the semigeostrophic approximation are believed to remain valid except in the immediate vicinity of the breakdown (Cullen and Purser 1984). The fields shown in Fig. 3 refer to physical (x, z) coordinates and represent vertical and horizontal cross sections of the relevant fields at successive times. The important characteristics of this solution have been well documented elsewhere but for future reference we list what we believe to be the most important physical aspects:

1) *Extremal values.* The fields Φ, v_g, θ, J, and u_{ag} all assume their maximum and minimum values along the horizontal boundaries $z = 0$, $z = 1$. The solutions corresponding to $q_g \equiv 0.0$ in the Eady model can therefore be interpreted as "boundary modes."

2) *Jacobian.* The maximum of J increases from 1.11 to 5.0 after 6.6 advection times. For Ro = 0.3 this corresponds to a dimensional time of 61 hours or 2.5 days. From the relation between the relative vorticity and the Jacobian, this corresponds to a relative vorticity of $4f$.

3) *Meridional geostrophic flow.* The maximum of v_g increases from 0.06 to 0.5 in the same time period. The dimensional maximum velocity at the final time occurs at the surfaces $Z = 0, 1$ and is 50 m s^{-1}. Regions with cyclonic vorticity (i.e., $\partial v_g/\partial x$ positive) have been contracted while anticyclonic regions have been expanded due to the advection by u_{ag}.

4) *Perturbation potential temperature.* The maximum of θ increases from 0.074 to approximately 0.57. In dimensional terms, this corresponds to an increase from 2.2 to 17 K. The temperature gradient across the frontal region near $x = 3$ is 30 K in 1000 km. The location of the zonal extrema for θ corresponds to the vertical extrema of v_g in accord with thermal wind balance.

5) *Ageostrophic winds.* The maximum of zonal ageostrophic velocity u_{ag} increases from 0.54 to 0.43 while the vertical velocity w increases from 0.018 to 0.16. In dimensional terms with Ro = 0.3, this corresponds to an increase in u_{ag} and w of 1.6 m s^{-1} to 13 m s^{-1} and 0.54 cm s^{-1} to 4.8 cm s^{-1}, respectively. The cross-frontal circulation is symmetric with regard to the strength of the ascent and descent velocities and also to the zonal ageostrophic velocities.

6) *Phase speed and growth rate.* The numerical simulation confirms a phase speed of 0.5 and a doubling time of 2.24 advection times.

In summarizing the classical frontogenesis solution we point out two important consequences of the uniform potential vorticity assumption. The first is that

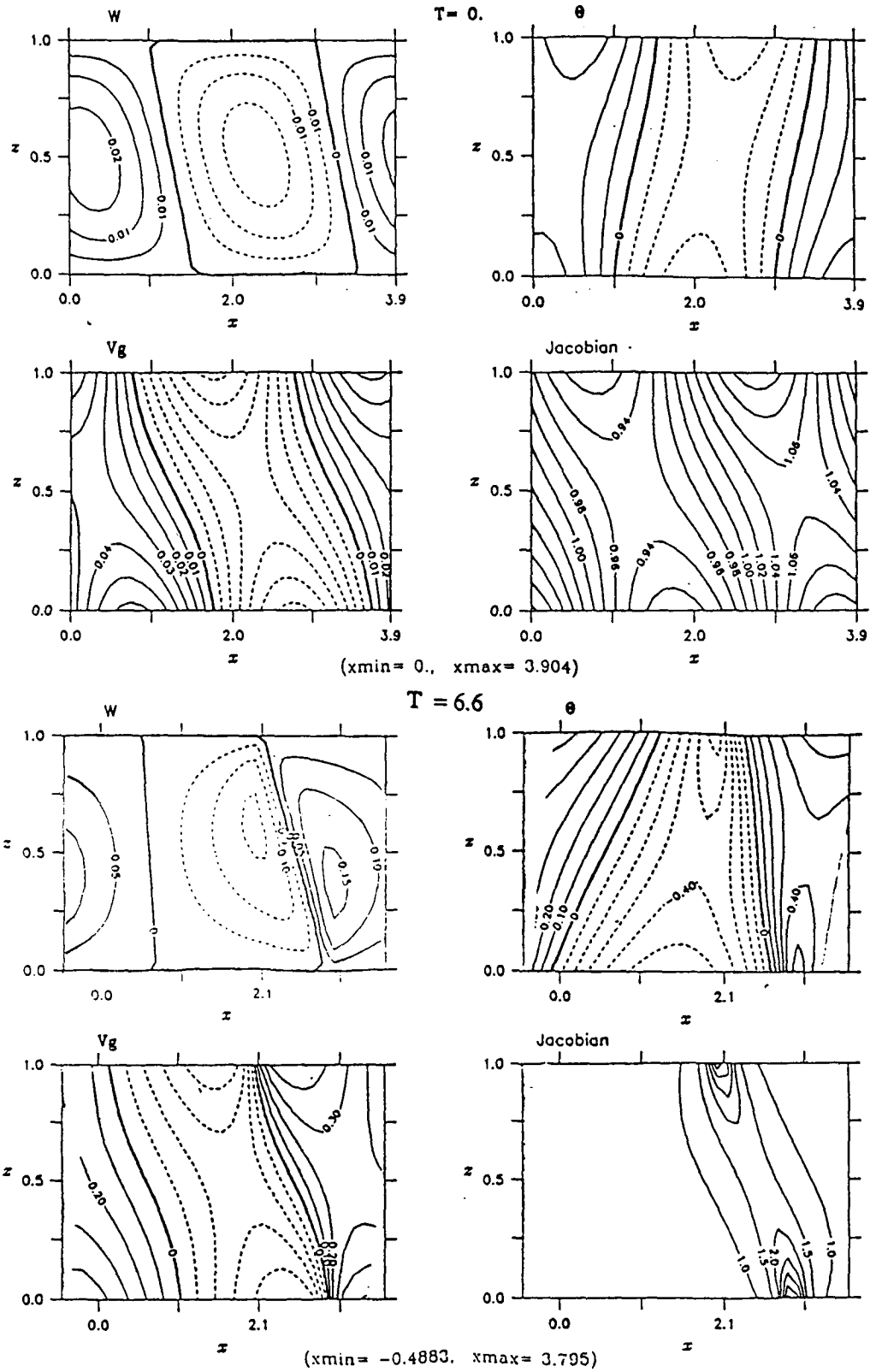

FIG. 3. Dynamics of the most unstable Eady mode with a zonal wavenumber $k = 1.61$. Shown are contour plots of w, θ, v_g and J at $T = 0$ and $T = 6.6$ nondimensional advection times with contour levels indicated on each plot. Solid lines denote positive values and dashed lines denote negative values. The minimum and maximum values of x given in parentheses at the bottom of each group of contour plots changes with time because of the geostrophic coordinate transformation $x = X - v_g(X, Z, T)$.

the system of equations becomes linear when expressed in the geostrophic coordinates thereby allowing superposition of elementary solutions. The second and physically interesting point is that for the exponentially growing solutions a singularity of the system (in the sense discussed above) is guaranteed regardless of the initial amplitude of the disturbance: one might have to wait a long time for a singularity to develop, but the exponential growth of the perturbation will eventually render the denominator in the Jacobian zero in finite time. For disturbances that have uniform potential vorticity and possess wavenumbers to the left of the short wave cutoff, the initial amplitude of the disturbance is not critical in determining whether a singularity will develop. On the other hand, as shown in the upcoming section for wave disturbances whose wavenumbers lie to the right of the short wave cutoff, the amplitude of the disturbance plays an important role in determining if the disturbance is capable of intensifying into a front.

4. Transient frontogenesis

When interior potential vorticity gradients are present in the model the classical frontogenetic solutions consisting solely of normal modes no longer comprise the general solution. For the Eady problem, Pedlosky (1964) showed that the normal modes of section 3 must be augmented by a continuous spectrum in order to completely represent a general disturbance. Observations show that the potential vorticity is not uniform in the troposphere and therefore frontogenesis models that assume uniform potential vorticity may neglect important physical processes. Mathematically speaking, there is a marked difference between uniform and nonuniform potential vorticity semigeostrophic flows. With uniform potential vorticity, the system (2.9) is linear in geostrophic space and the nonlinearity is implicit in the coordinate transformation back to real coordinates. However, in the nonuniform case the system (2.9) is explicitly nonlinear due to vertical advection of potential vorticity and also because the potential vorticity plays the same role as the static stability in both balance equations (2.9c, 2.9d).

The physical importance of potential vorticity anomalies have been discussed by Farrell (1984). In the Eady problem it was shown that the continuous spectrum gives rise to transient baroclinic development which can be rapid. For disturbances whose wavenumbers lie to the left of the short wave cutoff the transient solutions can have instantaneous growth rates much greater than the exponentially growing modes although in the (linear) quasi-geostrophic problem the exponential solutions dominate the $t \to \infty$ asymptotic limit. In Farrell (1984), it was argued that explosive cyclogenesis results from such transient processes stressing the initial value approach to understanding baroclinically developing systems. With a few simple examples, we explore some of the dynamical consequences of transient baroclinic development when q_g is nonzero in the frontogenetic two-dimensional Eady initial value problem.

A configuration commonly observed to precede explosive cyclogenesis consists of a positive upper-level potential vorticity disturbance upshear of a positive potential vorticity disturbance near the surface. The Presidents' Day Storm of Februrary 1979 is a well-documented example of explosive cyclogenesis following an initial flow configuration of this type. Observational accounts of this storm can be found in the works of Bosart (1981) and a recent numerical study by Whitaker et al. (1988). An initial configuration of this kind is qualitatively represented by a plane wave disturbance in the geopotential Φ leaning approximately 50 degrees from the z axis against the shear and is similar to the one discussed by Farrell (1984). The perturbation is:

$$\Phi(X, Z, 0) = \Phi_{\text{amp}} \sin(kX + mZ) \qquad (4.1)$$

Figure 4 corresponds to a simulation with $k = 2.5$, $m = 3.0$ and $\Phi_{\text{amp}} = 0.025$. From Fig. 1, this choice of k lies slightly to the right of the short wave cut-off beyond which there are no exponentially unstable modes. Dimensional values implied by this choice of parameters are meridional wind speeds v_g and potential temperature disturbances θ of approximately 6 m s^{-1} and 2 K. The strength of this disturbance is therefore comparable to the normal mode disturbance of section 3. The salient features of the solution are discussed below.

1) *Potential vorticity.* The potential vorticity anomaly q_g generally follows the mean flow and is sheared, although advection by both u_{ag} and w strongly distorts the initial plane wave structure.

2) *Extremal values.* The initial fields Φ, v_g, θ and J do not assume their maximal values on the horizontal boundaries as in the case of a normal mode but are constant along the lines $kx + mz$ = constant. After 2.8 advection times, corresponding to a dimensional time of approximately 25 hours, these fields become most intense at the horizontal boundaries and look qualitatively similar to a superposition of upper and lower normal modes whose upper mode is displaced upstream of the lower one.

3) *Jacobian.* The maximum of J increases from 1.15 to 10.0 after 2.8 advection times. This corresponds to a relative vorticity of $9f$.

4) *Meridional geostrophic flow.* The maximum of v_g increases from 0.06 to 0.38 along the horizontal boundaries in the same time period and results in a final dimensional velocity of 38 m s^{-1}. The differential in velocity across the front at $x = 0.5$ is nearly 70 m s^{-1}.

5) *Perturbation potential temperature.* The maximum of θ (not shown) increases from 0.06 to 0.39 in the same time period corresponding to an increase from

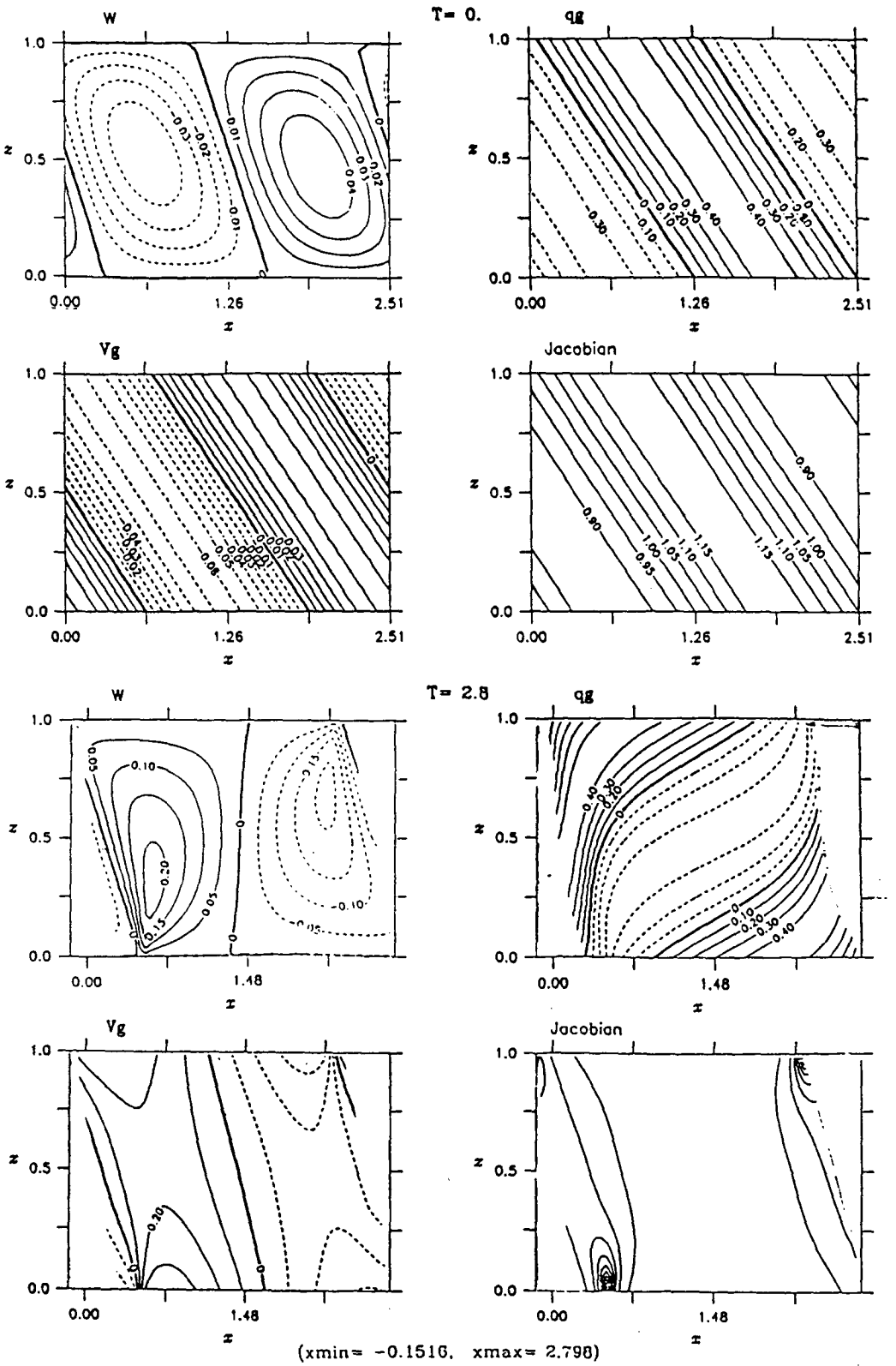

FIG. 4. Dynamics of the plane wave initial condition (4.1) with a zonal wavenumber $k = 2.5$. Shown are contour plots of w, q_g, v_g and J at $T = 0.$ and $T = 2.8$ nondimensional advection times with contour levels indicated on each plot. Solid lines denote positive values and dashed lines denote negative values. The minimum and maximum values of x given in parentheses at the bottom of each group of contour plots changes with time because of the geostrophic coordinate transformation $x = X - v_g(X, Z, T)$.

approximately 1.8 to 11.7 K. The temperature gradient across the frontal region near $x = 0.5$ is 20 K in 1300 km.

6) *Ageostrophic winds.* The maximum of u_{ag} increases from 0.08 to 0.42 while w increases from 0.04 to 0.22. This corresponds to an increase in u_{ag} from 2.4 m s^{-1} to 12 m s^{-1} and in increase in w from 1.2 cm s^{-1} to 6.6 cm s^{-1}. The cross-frontal circulation is symmetric with regard to the strength of the ascending and descending velocities and zonal ageostrophic winds.

7) *Growth rate.* For this choice of k there are no exponentially growing solutions and hence the modes excited by the initial condition (4.1) are entirely neutral in the exponential sense. Nevertheless the excited neutral modes rapidly intensify since, with phase aligned against the shear, they are properly configured to tap the available potential energy of the mean state. A crude growth rate for this solution can be obtained, for example, by simply assuming that the geostrophic wind v_g grows exponentially with a starting value of 0.06 and a final value of 0.38 at $t = 2.8$ advection times. This simple calculation gives a growth rate of approximately 0.66, which is more than twice the maximum growth rate for the Eady normal modes. Despite the lack of exponentially growing normal modes for this disturbance, the neutral modes develop rapidly into a mature front.

The system (2.9–2.10) generally has a dependence on the amplitude of the geopotential Φ. This is easily illustrated for the current example by integrating the same initial condition (4.1) with a ninety percent reduction in amplitude: $\Phi_{amp} = 0.0025$. The results of integrating the model with this reduced initial condition are shown in Fig. 5. The results shown correspond to $T = 7.7$ and all fields refer to physical (x, z) coordinates. The most interesting features are:

1) *Potential vorticity.* The potential vorticity field q_g follows the mean flow and is sheared. The zonal and vertical advection of potential vorticity is practically absent with not much distortion of q_g phase lines.

2) *Jacobian.* The maximum in the Jacobian increased from 1.011 to only 1.2 after 8 advection times. This implies a relative vorticity maximum of $0.2f$ located along the horizontal boundaries.

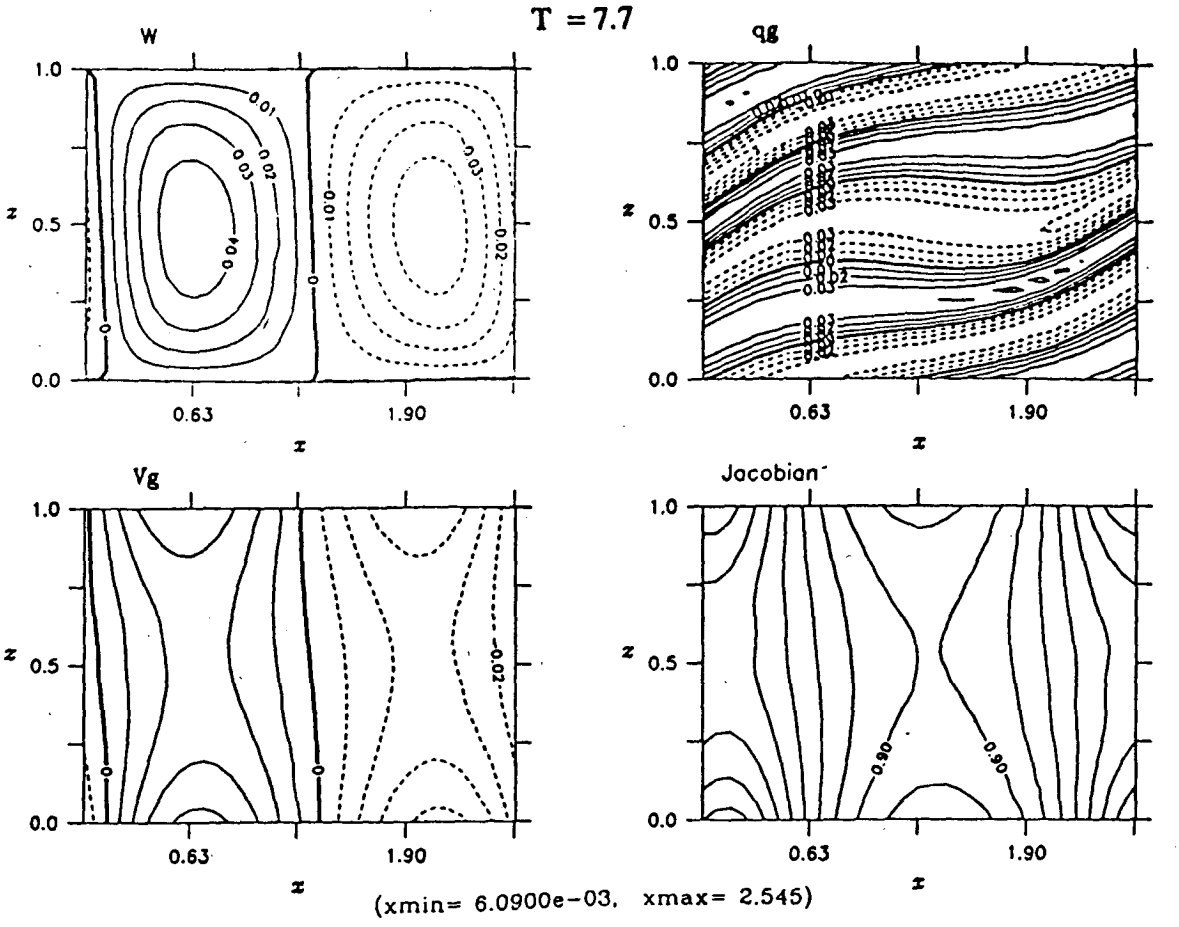

FIG. 5. Resultant fields at $T = 7.7$ nondimensional advection times for the plane wave initial condition of Fig. 4 reduced by 10 in magnitude.

3) *Phase structure.* From the contour plot for v_g it is clear that the baroclinic growth stage for this perturbation is complete since it is aligned almost vertically and no longer properly configured to extract available potential energy from the mean state. The solution structure is qualitatively the same as in the first example resembling a superposition of an upper and lower neutral mode. At subsequent times the upper mode passes the lower mode.

In order for neutral disturbances to intensify into a mature front, the strength of the initial disturbance must be sufficiently great. How to choose the initial amplitude to render the transformed relative vorticity $\partial v_g/\partial X = f$ at some later time by inspection is not obvious since 1) these solutions have ever changing structures and 2) the growth of relative vorticity results after baroclinic conversion of available potential energy to perturbation energy. However, as shown in the first example, these initial disturbances did not require unusually high amplitudes.

The third example addresses the structural aspect of the q_g anomaly used as an initial condition. Recently Farrell (1989) formulated the problem of finding perturbations that optimally excite a chosen mode as a variational problem. For exciting the lower level Eady neutral mode at zonal wavenumber k to the right of the short wave cutoff, a near optimal initial condition in the energy norm is given by the approximate adjoint of the mode:

$$\Phi_{\text{opt}} = \text{Re}\left[\frac{\Phi(X, Z, k, c_r, c_i \equiv 0; T = 0)}{(Z - (c_r + i\delta))}\right] \quad (4.3)$$

where $\Phi(\cdots)$ denotes a neutral normal mode as defined in section 3. A wavenumber of $k = 3$ is chosen and δ is a nonzero parameter taken to equal -0.15 in this example. The main effect of δ is simply to control the tilt angle that the perturbation makes with the z axis.

The initial fields consistent with this disturbance are plotted at the top of Fig. 6a. The maximum of q_g is 0.59 and the minimum is -0.53. The dimensional values of v_g and θ are 1.9 m s^{-1} and 1.26 K, respectively. The results of the integration at successive times are shown in Fig. 6a and Fig. 6b, at 36 and 54 hours, with fields referred to physical (x, z) coordinates and are discussed below.

1) *Jacobian and potential vorticity.* The maximum of J is 10.0 at 6.1 advection times and it occurs on the lower surface near $x = 0.9$. This implies a relative vorticity of $9f$. The potential vorticity anomaly generally follows the mean flow and is sheared as shown at 4 advection times; the advection by the vertical and zonal velocities is beginning to distort the anomaly by raising the region where q_g is negative and lowering the region where q_g is positive. At 6.1 advection times the negative anomaly has almost rolled on top of the positive anomaly with the latter being pushed downward into the lower surface $z = 0$.

2) *Extremal values.* The extremal values of the initial fields Φ, q_g, v_g, J, θ and w are located along the line given by $Z = 0.338$ that corresponds to the location of the extrema of the geopotential. At 4 advection times the extrema in the fields Φ, v_g, J, θ and u_{ag} occur only on the lower surface $Z = 0$. From the plot of v_g at 4 advection times, the disturbance along the lower surface is qualitatively similar to a lower neutral (normal) mode although there is much more structure evident. At 6.1 advection times the initial disturbance has intensified to frontal strength and the extremal values are located on the lower surface. By this time there is a relatively weak disturbance along the upper surface and the resemblance of a lower neutral normal mode persists despite distortions by ageostrophic winds.

3) *Meridional geostrophic flow and perturbation potential temperature field.* The maximum of v_g increases from 0.019 to 0.26 at $T = 6.1$ resulting in a final dimensional velocity of 26 m s^{-1}. The differential in velocity across the front is approximately 45 m s^{-1}. The magnitude of θ (not shown) increases from 0.04 to 0.27 in the same time period corresponding to an increase from 1.2 to 8.1 K. The temperature gradient across the frontal region is 15 K in 800 km.

4) *Ageostrophic winds.* The maximum of u_{ag} increases from 0.024 to 0.25 while w increases from 0.01 to 0.145. In dimensional terms with Ro = 0.3, this corresponds to an increase in u_{ag} from 0.72 m s^{-1} to 7.5 m s^{-1} and an increase in w from 0.3 cm s^{-1} to 4.35 cm s^{-1}. The strengths of the ascending and descending regions are approximately equal and the vertical location of $w_{\max}$ and $w_{\min}$ is along the line $Z = 0.33$.

5) *Phase structure and growth rate.* The contour plot for v_g at 6.1 advection times shows a structure slightly tilted against the shear that would, if continued, extract an additional small amount of available potential energy from the mean state. The integration for this example was not continued beyond 6.1 advection times. As in the first example, there are no exponentially growing solutions for $k = 3$ and hence the modes excited by the initial condition (4.3) are entirely neutral in the exponential sense. This predominantly lower-level neutral wave rapidly intensifies since its phase tilts against the shear and is therefore properly configured to tap the available potential energy present in the mean state. Once again, a crude growth rate for this solution is obtained simply by assuming that the geostrophic wind v_g grows exponentially with a starting value of 0.02 and a final value of 0.26 at $t = 6.1$ advection times. This simple calculation gives a growth rate of approximately 0.42, which is nearly thirty percent greater than the maximum growth rate for the Eady normal modes. Thus, despite the lack of exponentially growing normal modes for this energetically near optimal disturbance, the neutral modes develop rapidly into a mature front.

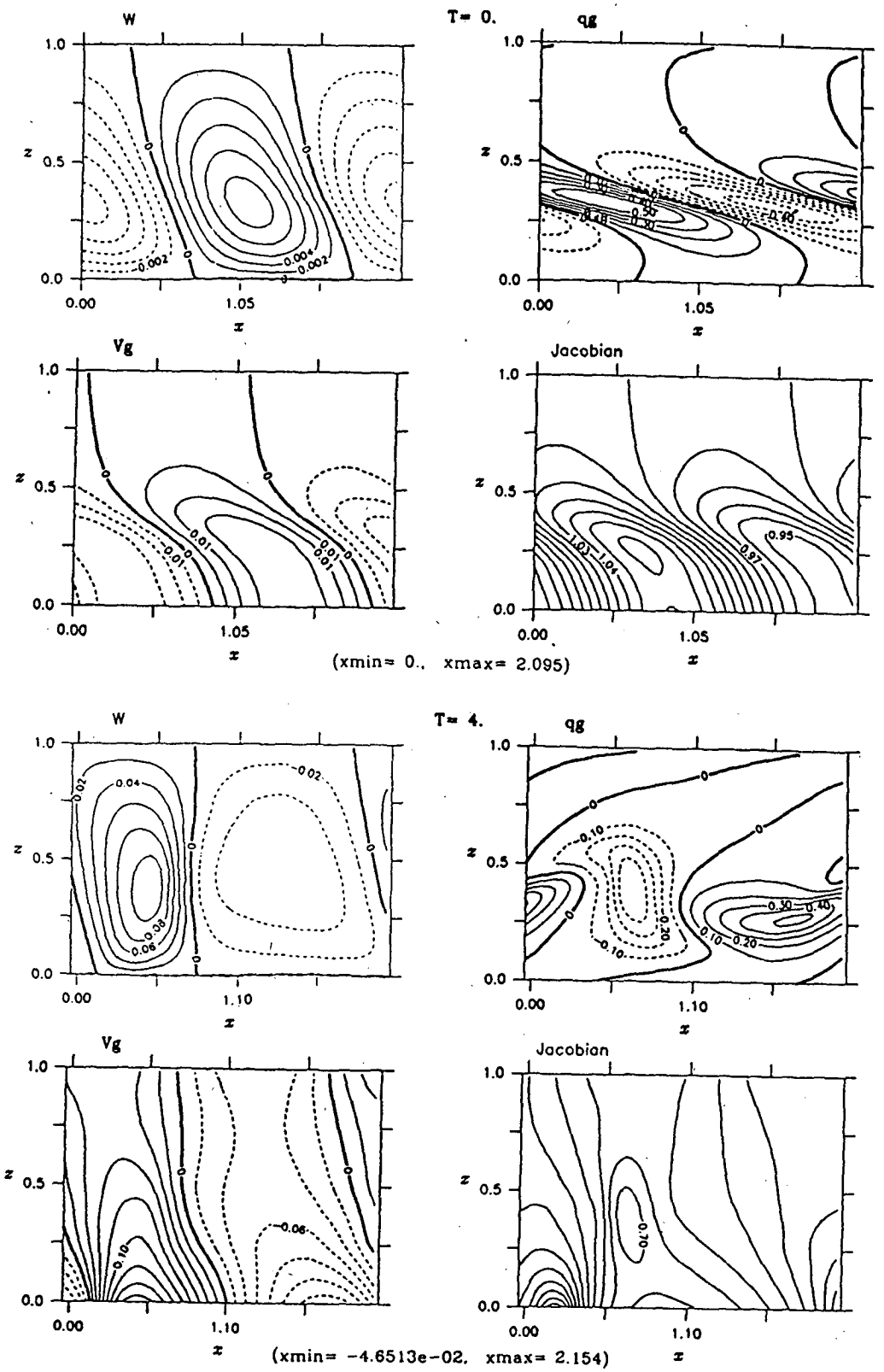

FIG. 6a. Dynamics of the energetic optimal disturbance defined by (4.3) with a zonal wavenumber $k = 3$. Shown are contour plots of w, q_g, v_g and J with contour levels indicated on each plot. Solid lines denote positive values and dashed lines denote negative values. The minimum and maximum values of x given in parentheses at the bottom of each group of contour plots changes with time because of the geostrophic coordinate transformation $x = X - v_g(X, Z, T)$.

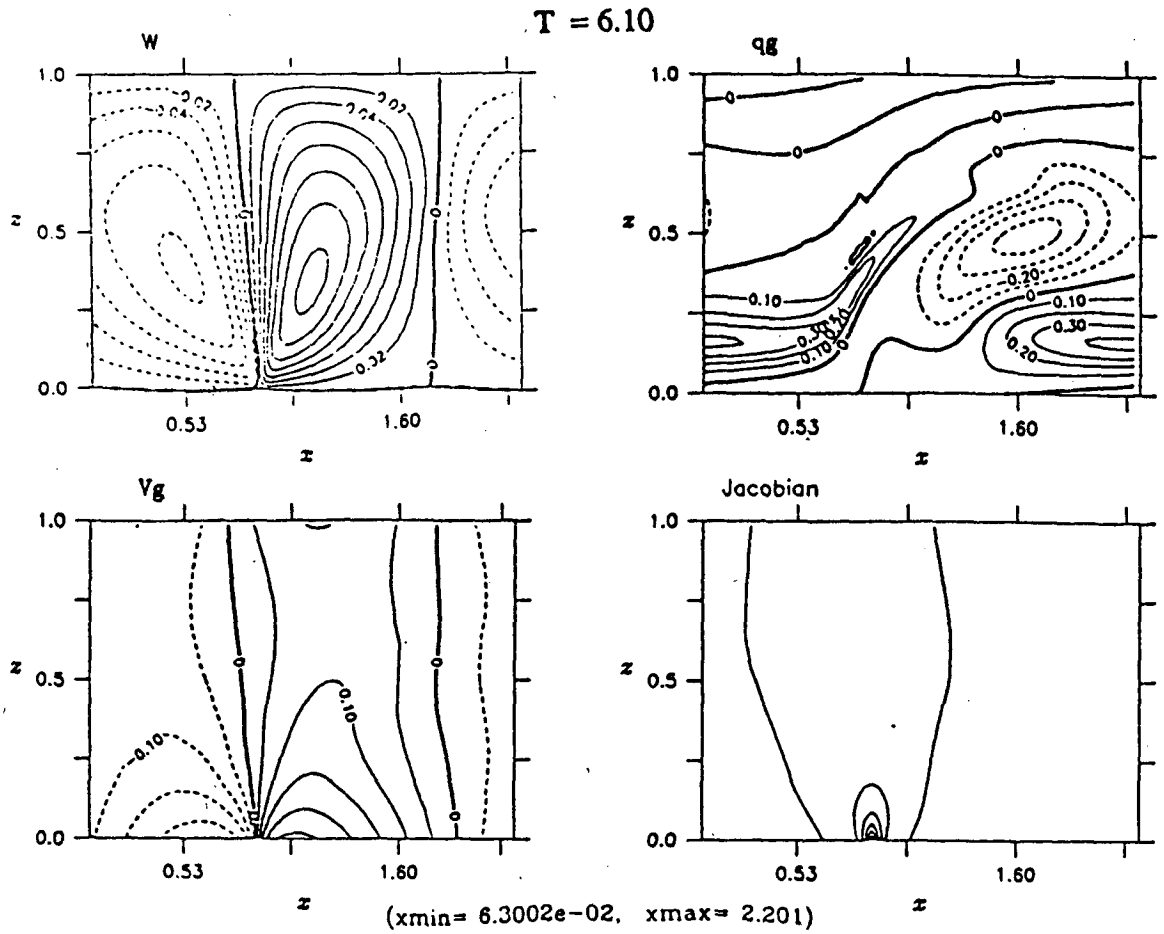

FIG. 6b. Same as in Fig. 6a but shown are the resultant fields at $T = 6.1$ nondimensional advection times for the optimal disturbance defined by (4.3) with a zonal wavenumber $k = 3$.

As a final example consider the same initial condition (4.3) keeping $\delta = -0.15$, but this time increasing the zonal wavenumber to $k = 6$. In this case $c_r = 0.167$ and the amplitude is chosen to give a dimensional v_g surface maximum of 3.8 m s^{-1} and a nondimensional q_g maximum of 0.46. The maximum of the potential vorticity field occurs along the line $Z \approx 0.16$. The dynamics are summarized in Fig. 7 where we show the fields (w, q_g, v_g and J) at $T = 0$, and three nondimensional advection times. The behavior is similar to the previous example except that the maximum in the w field occurs much closer to the lower surface. The Jacobian at $T = 4$ is 12.1 corresponding to a relative vorticity of $11.1f$ with 25 m s^{-1} across the cyclonic vorticity frontal zone. The maximum ascending velocity increases from 0.5 cm s^{-1} to 1.93 cm s^{-1} by four advection times and is located along the line $Z = 0.16$. Like the previous example this disturbance produces a modest frontal zone despite the lack of sustained exponential growth.

Previous investigations (Hoskins and Bretherton 1972) focused only on the most rapidly growing exponential normal mode that gives vertical velocity maxima, w_{max}, in the midtroposphere. Subsequent investigators (Blumen 1979; Mak and Bannon 1984) considered boundary layer frictional convergence and diabatic processes in an attempt to account for the intensity and near surface location of w_{max} above frontal zones—common characteristics of surface fronts (Sanders 1983). However, even with the inviscid dry model we find that the location of w_{max} above a frontal zone need not always occur in the midtroposphere. Specifically, for nonuniform potential vorticity flows the location of w_{max} is a strong function of the vertical structure of the interior potential vorticity field. In both of the above examples the vertical location of w_{max} coincides with the maximum of q_g and is near the lower surface.

5. Discussion and conclusion

The intensification of baroclinic disturbances with nonuniform potential vorticity into surface frontal systems has been examined for the two-dimensional semigeostrophic Eady initial value problem. Of the four initial conditions presented in section 4, three devel-

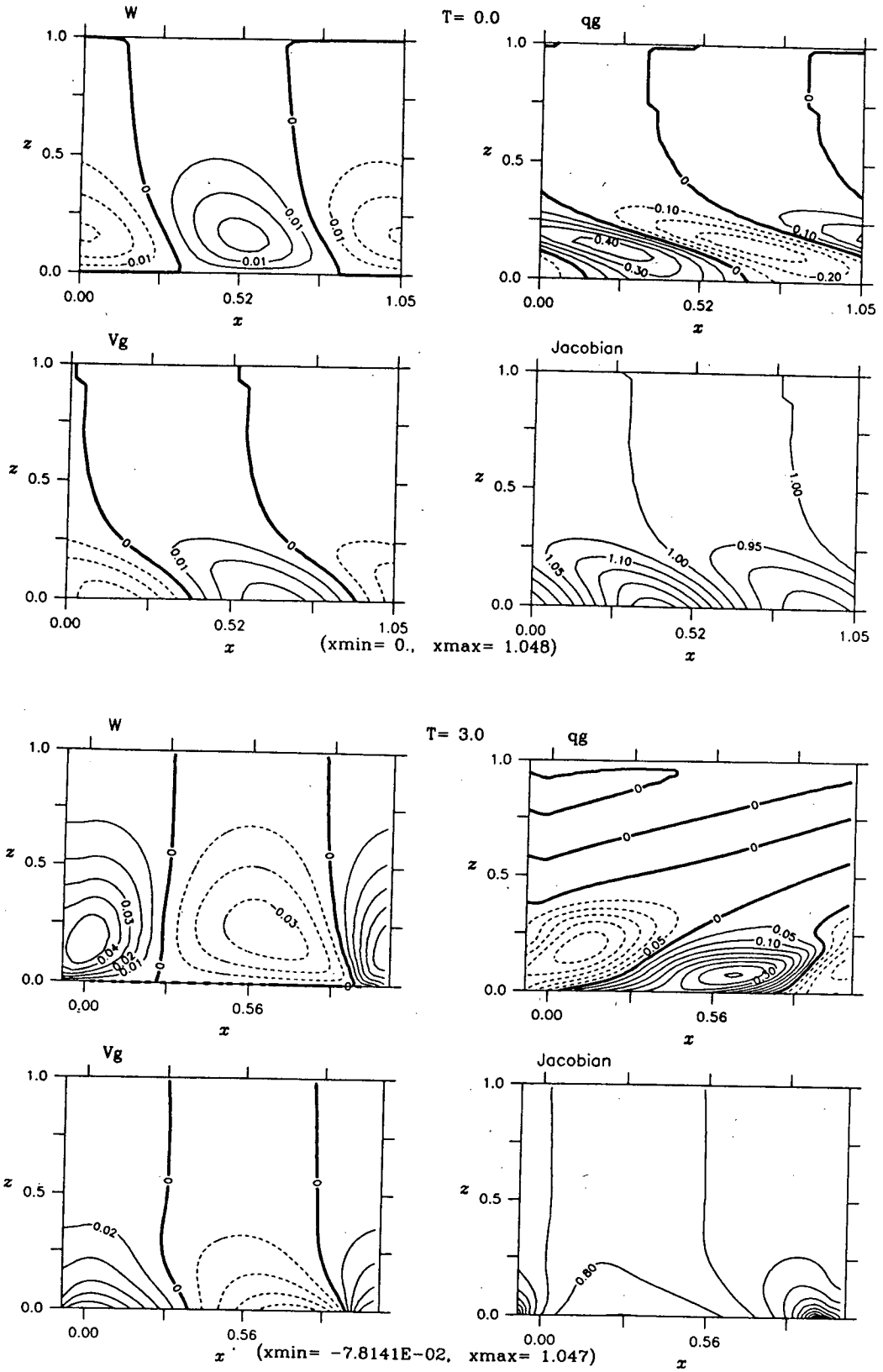

FIG. 7. Dynamics of the energetic approximate optimal disturbance defined by (4.3) with zonal wavenumber $k = 6$. Solid lines denote positive values and dashed lines denote negative values. The minimum and maximum x values given in parentheses at the bottom of each group of contour plots changes with time because of the geostrophic coordinate transformation $x = X - v_g(X, Z, T)$.

oped into mature surface fronts. The disturbances chosen had zonal wavenumbers exceeding the short wave cutoff so that no exponentially growing solutions were present. Lack of exponential growth for these disturbances did not hinder frontal development but instead required the strength of the disturbance exceed an amplitude threshold. In practice, however, the finite amplitude constraint required for surface front formation is not severe as illustrated by the examples of section 4. The location of the vertical velocity maxima above the surface frontal zone is found to depend upon the vertical structure of the potential vorticity field. The latter two examples exhibit vertical velocity maxima near the lower surface. For disturbances having wavenumbers to the left of the short wave cutoff the solution may comprise two phases. The first phase is a transient growth that is replaced in the second phase by exponential growth in the $t \rightarrow \infty$ limit. In the semigeostrophic Eady model the rapidity of the transient development illustrated in section 4 suggests, even for these wavenumbers, that moderately strong disturbances could intensify into a strong front before transition to the exponential growth phase.

The model results reported in section 4 motivates further frontogenesis research using the initial value approach. For example, a problem of both physical and mathematical interest is to formulate a variational analogue of the energetic optimal problem for frontogenesis. The problem would be to determine the disturbance that yields maximum frontogenesis (i.e., large relative vorticity) in a given time period.

The model used in this paper has limitations of which perhaps the most important are:

(i) the neglect of wave mean flow interactions
(ii) the neglect of moisture in the lower atmosphere
(iii) the neglect of friction along the horizontal surfaces.

The two-dimensional Eady model precludes all interaction of the disturbances with the mean flow. For a more realistic three-dimensional problem there generally will be a change in the basic state as the disturbances extract available potential energy from it. This interaction would modify the instantaneous growth rate of the disturbances and could significantly alter the resulting frontal structures formed.

Recent work on the effect of moisture in the two-dimensional Eady problem (Emanuel et al. 1987) demonstrates the increase of growth rate, destabilization of waves near the short wave cutoff, and intensification of the ascending vertical velocity due to release of latent heat as moist air is lifted and condenses. In this paper, we considered the dynamics of dry air on the grounds that a full understanding of the dynamics associated with dry potential vorticity anomalies at finite amplitude was lacking. An important direction for future study is to include the effects of moisture.

The final limitation of the model concerns the lower surface boundary condition. Significant progress has been made (Blumen and Wu 1982, 1983) for the semigeostrophic balance approximation in formulating a self-consistent boundary condition that would be applied at the top of an Ekman layer. Inclusion of an Ekman layer in the traditional Charney model along the rigid boundary $Z = 0$ leads to important changes in the growth rates of the exponentially unstable modes (Farrell 1985). Depending on the value of the effective viscosity, the growth rates may be significantly reduced. For instance, with values of the effective viscosity on the order of 5 $m^2 s^{-1}$, the maximum growth rate at wavelengths of 3000 km is reduced to zero, but Farrell (1985) demonstrated the robust behavior of transient baroclinic development and showed its insensitivity to the presence of an Ekman layer. Similarly, the addition of Ekman pumping in the Eady model significantly reduces the growth rates of exponentially growing solutions although the transient modes continue to exhibit rapid baroclinic development. Applying this reasoning to the damped frontogenesis model suggests that transient solutions would be the predominant frontogenetic agents. However, it is clear that the presence of an Ekman layer at the lower surface would raise the amplitude threshold determining whether a front will form since the disturbances would have to overcome frictional dissipation in the boundary layer.

The importance of the initial value problem is that it allows exploration of a great variety of possible frontal developments, permitting study of both amplitude and structural sensitivity of disturbances leading to frontogenesis. The two-dimensional semigeostrophic Eady model is the accepted paradigm for surface frontogenesis in association with intensifying baroclinic waves. Surface fronts presented here are characterized by strong horizontal wind shears but have relatively weak thermal contrasts across them. Nevertheless, despite the Eady model's inability to produce strong thermal contrasts, it is a simple phenomenological model for understanding the previously unexplored role of interior potential vorticity in dry surface frontogenesis. Further observations of tropospheric potential vorticity anomalies are indicated to determine realistic potential vorticity structures, the dynamics of which are central to the formation of atmospheric fronts.

Acknowledgments. This work was supported by NSF ATM-8712995 and ATM-8912432.

REFERENCES

Bjerknes, J., 1919: On the structure of moving cyclones. *Geofys. Publ.*, **1**, 1–8.
——, and E. Palmen, 1937: Investigations of selected European cyclones by means of serial ascents. *Geofys. Publ.*, **12**, 1–62.
Blumen, W., 1979: A comparison between the Hoskins-Bretherton model of frontogenesis and the analysis of an intense surface frontal zone. *J. Atmos. Sci.*, **37**, 64–77.
——, and R. Wu, 1982: An analysis of Ekman boundary layer dynamics incorporating the geostrophic momentum approximation. *J. Atmos. Sci.*, **39**, 1774–1782.
——, and ——, 1983: Baroclinic instability and frontogenesis with

Ekman boundary layer dynamics incorporating the geostrophic momentum approximation. *J. Atmos. Sci.*, **40**, 2630–2637.

Bosart, L. F., 1981: The Presidents' Day Snowstorm of 18–19 February 1979: A subsynoptic scale event. *Mon. Wea. Rev.*, **109**, 1542–1566.

Charney, J., 1947: The dynamics of long waves in a baroclinic westerly current. *J. Meteor.*, **4**, 125–162.

Cullen, M. J. P., and R. J. Purser, 1984: An extended lagrangian theory of semi-geostrophic frontogenesis. *J. Atmos. Sci.*, **41**, 1477–1497.

Eady, E. J., 1949: Long waves and cyclone waves. *Tellus*, **1**, 33–52.

Eliassen, A., 1962: On the vertical circulations in frontal zones. *Geofys. Publ.*, **24**(4), 147–160.

——, and E. Kleinschmidt, 1957: Dynamic meteorology. Handbuch der Physik, Vol. 48, Springer Verlag, 1–154.

Emanuel, K. A., M. Fantini and A. J. Thorpe, 1987: Baroclinic instability in an environment of small stability to slantwise moist convection. Part I: Two-dimensional models. *J. Atmos. Sci.*, **44**, 1559–1573.

Farrell, B. F., 1984: Modal and non-modal baroclinic waves. *J. Atmos. Sci.*, **41**, 668–673.

——, 1985: Transient growth of damped baroclinic waves. *J. Atmos. Sci.*, **42**, 2718–2727.

——, 1989: Optimal excitation of baroclinic waves. *J. Atmos. Sci.*, **46**, 1193–1206.

Hoskins, B. J., 1975: The geostrophic momentum approximation and the semigeostrophic equations. *J. Atmos. Sci.*, **32**, 233–242.

——, and F. P. Bretherton, 1972: Atmospheric frontogenesis models: Mathematical formulation and solution. *J. Atmos. Sci.*, **29**, 11–37.

——, and I. Draghici, 1977: The forcing of ageostrophic motion according to the semigeostrophic equations and in an isentropic coordinate model. *J. Atmos. Sci.*, **34**, 1859–1867.

——, M. E. McIntyre and A. W. Robertson, 1985: On the use and significance of potential vorticity maps. *Quart. J. Roy. Meteor. Soc.*, **111**, 877–946.

Mak, M., and P. R. Bannon, 1984: Frontogenesis in a moist semigeostrophic model. *J. Atmos. Sci.*, **41**, 3485–3500.

Palmen, E., and C. W. Newton, 1948: A study of the mean wind and temperature distribution in the vicinity of the polar front in winter. *J. Meteor.*, **5**, 220–226.

Pedlosky, J., 1964: An initial-value problem in the theory of baroclinic instability. *Tellus*, **16**, 12–17.

Sanders, F., 1955: An investigation of the structure and dynamics of an intense surface frontal zone. *J. Meteor.*, **12**, 542–552.

——, 1983: Observations of Fronts. *Mesoscale Meteorology*, D. Reidel, 781 pp.

Whitaker, J. S., L. W. Uccellini, K. F. Brill, 1988: A model-based diagnostic study of the rapid development phase of the Presidents' Day cyclone. *Mon. Wea. Rev.*, **116**, 2337–2365.

Williams, R. T., 1967: Atmospheric frontogenesis: A numerical experiment. *J. Atmos. Sci.*, **24**, 627–641.

——, and J. Plotkin, 1968: Quasi-geostrophic frontogenesis. *J. Atmos. Sci.*, **25**, 201–206.